Search for $K^+ \to \pi^+ \nu \bar{\nu}$ at the NA62 experiment

Viacheslav Duk[1],[⋆] for the NA62 collaboration [⋆⋆]

[1]*INFN Perugia, Italy*

Abstract. Looking for phenomena beyond the Standard Model (SM) in rare decays is a complementary approach to direct searches for New Physics (NP) at colliders. One of the theoretically cleanest processes is the ultra rare decay $K^+ \to \pi^+ \nu \bar{\nu}$. The goal of the NA62 experiment at CERN SPS is to measure the branching ratio (BR) of this decay with 10% precision. The experiment has been launched in 2014. In 2015, the detector was commissioned at a low intensity beam. The experimental setup is described and performances achieved in 2015 are discussed in view of the final measurement.

1 $K \to \pi \nu \bar{\nu}$ decays

The ultra rare decays $K^+ \to \pi^+ \nu \bar{\nu}$ and $K_L \to \pi^0 \nu \bar{\nu}$ proceed via flavor changing neutral currents (FCNC) and are highly suppressed in the SM due to the GIM mechanism. The Feynman diagrams of box and penguin contributions are shown in Fig. 1.

[⋆]e-mail: Viacheslav.Duk@cern.ch
[⋆⋆]G. Aglieri Rinella, R. Aliberti, F. Ambrosino, R. Ammendola, B. Angelucci, A. Antonelli, G. Anzivino, R. Arcidiacono, I. Azhinenko, S. Balev, M. Barbanera, J. Bendotti, A. Biagioni, L. Bician, C. Biino, A. Bizzeti, T. Blazek, A. Blik, B. Bloch-Devaux, V. Bolotov, V. Bonaiuto, M. Boretto, M. Bragadireanu, D. Britton, G. Britvich, M.B. Brunetti, D. Bryman, F. Bucci, F. Butin, E. Capitolo, C. Capoccia, T. Capussela, A. Cassese, A. Catinaccio, A. Cecchetti, A. Ceccucci, P. Cenci, V. Cerny, C. Cerri, B. Checcucci, O. Chikilev, S. Chiozzi, R. Ciaranfi, G. Collazuol, A. Conovaloff, P. Cooke, P. Cooper, G. Corradi, E. Cortina Gil, F. Costantini, F. Cotorobai, A. Cotta Ramusino, D. Coward, G. D'Agostini, J. Dainton, P. Dalpiaz, H. Danielsson, J. Degrange, N. De Simone, D. Di Filippo, L. Di Lella, S. Di Lorenzo, N. Dixon, N. Doble, B. Dobrich, V. Duk, V. Elsha, J. Engelfried, T. Enik, N. Estrada, V. Falaleev, R. Fantechi, V. Fascianelli, L. Federici, S. Fedotov, M. Fiorini, J. Fry, J. Fu, A. Fucci, L. Fulton, S. Gallorini, S. Galeotti, E. Gamberini, L. Gatignon, G. Georgiev, A. Gianoli, M. Giorgi, S. Giudici, L. Glonti, A. Goncalves Martins, F. Gonnella, E. Goudzovski, R. Guida, E. Gushchin, F. Hahn, B. Hallgren, H. Heath, F. Herman, T. Husek, O. Hutanu, D. Hutchcroft, L. Iacobuzio, E. Iacopini, E. Imbergamo, O. Jamet, P. Jarron, E. Jones, T. Jones K. Kampf, J. Kaplon, V. Kekelidze, S. Kholodenko, G. Khoriauli, A. Khotyantsev, A. Khudyakov, Yu. Kiryushin, A. Kleimenova, K. Kleinknecht, A. Kluge, M. Koval, V. Kozhuharov, M. Krivda, Z. Kucerova, Yu. Kudenko, J. Kunze, G. Lamanna, G. Latino, C. Lazzeroni, G. Lehmann-Miotto, R. Lenci, M. Lenti, E. Leonardi, P. Lichard, R. Lietava, L. Litov, R. Lollini, D. Lomidze, A. Lonardo, M. Lupi, N. Lurkin, K. McCormick, D. Madigozhin, G. Maire, C. Mandeiro, I. Mannelli, G. Mannocchi, A. Mapelli, F. Marchetto, R. Marchevski, S. Martellotti, P. Massarotti, K. Massri, P. Matak, E. Maurice, A. Mefodev, E. Menichetti, E. Minucci, M. Mirra, M. Misheva, N. Molokanova, J. Morant, M. Morel, M. Moulson, S. Movchan, D. Munday, M. Napolitano, I. Neri, F. Newson, A. Norton, M. Noy, G. Nuessle, T. Numao, V. Obraztsov, A. Ostankov, S. Padolski, R. Page, V. Palladino, G. Paoluzzi, C. Parkinson, E. Pedreschi, M. Pepe, F. Perez Gomez, M. Perrin-Terrin, L. Peruzzo, P. Petrov, F. Petrucci, R. Piandani, M. Piccini, D. Pietreanu, J. Pinzino, I. Polenkevich, L. Pontisso, Yu. Potrebenikov, D. Protopopescu, F. Raffaelli, M. Raggi, P. Riedler, A. Romano, G. Ruggiero, V. Russo, V. Ryjov, A. Salamon, G. Salina, V. Samsonov, C. Santoni, G. Saracino, F. Sargeni, V. Semenov, M. Serra, A. Sergi, M. Serra, A. Shaikhiev, S. Shkarovskiy, I. Skillicorn, D. Soldi, A. Sotnikov, V. Sugonyaev, M. Sozzi, T. Spadaro, F. Spinella, R. Staley, A. Sturgess, P. Sutcliffe, N. Szilasi, D. Tagnani, S. Trilov, M. Valdata-Nappi, P. Valente, M. Vasile, T. Vassilieva, B. Velghe, M. Veltri, S. Venditti, P. Vicini, R. Volpe, M. Vormstein, H. Wahl, R. Wanke, P. Wertelaers, A. Winhart, R. Winston, B. Wrona, O. Yushchenko, M. Zamkovsky, A. Zinchenko.
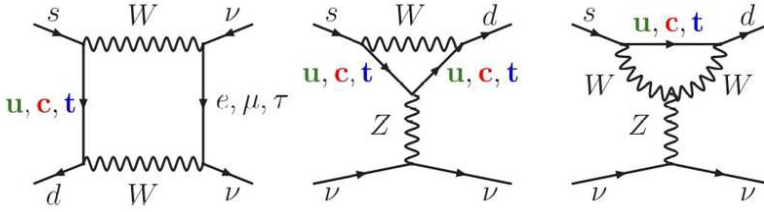
Figure 1. Box and penguin diagrams contributing to $K \to \pi\nu\bar{\nu}$ decays.

Within the SM, BR theoretical values contain CKM matrix elements as external inputs. These elements give the largest uncertainty to the BR. Using tree-level observables, one obtains [1, 2]:

$$BR(K^+ \to \pi^+\nu\bar{\nu}) = (8.4 \pm 1.0) \times 10^{-11} \ ,$$

$$BR(K_L \to \pi^0\nu\bar{\nu}) = (3.4 \pm 0.6) \times 10^{-11} \ .$$

These values are not polluted by contributions from the NP and hence are suitable for a NP search as a deviation from the SM BR value. More precise calculation with the loop-level measurements of the CKM elements assumes the absence of NP and provides the best accuracy for further recalculation of CKM elements from the comparison of theoretical and experimental BR values:

$$BR(K^+ \to \pi^+\nu\bar{\nu}) = (9.1 \pm 0.7) \times 10^{-11} \ ,$$

$$BR(K_L \to \pi^0\nu\bar{\nu}) = (3.0 \pm 0.3) \times 10^{-11} \ .$$

$K \to \pi\nu\bar{\nu}$ decays are very sensitive to NP. The largest contribution to the BR could come from models with new sources of flavor violation [3, 4]. The 10% precision measurement of the BR will allow to probe NP at mass scales up to 100 TeV.

The only experimental measurement in the charged mode based on the observation of 7 events and decay-at-rest technique has been performed by the E787 and E949 experiments [5], while for the neutral mode there is only an upper limit on the BR from the E391 collaboration [6]:

$$BR(K^+ \to \pi^+\nu\bar{\nu}) = (17.3^{+11.5}_{-10.5}) \times 10^{-11} \ ,$$

$$BR(K_L \to \pi^0\nu\bar{\nu}) < 2.6 \times 10^{-8} \ .$$

2 NA62 experiment

The NA62 experiment plans to collect 10^{13} kaon decays in the fiducial volume which corresponds to ~100 SM events of $K^+ \to \pi^+\nu\bar{\nu}$ with ~10% acceptance. The detailed description of the NA62 apparatus can be found in [7]. The schematic view of the setup is shown in Fig. 2.

A proton beam from CERN SPS (400 GeV/c) impinging on a Beryllium target produces a secondary hadron beam of 75 GeV/c with ~6% of K^+. Kaons are identified by the CEDAR detector (**KTAG**), a differential Cherenkov counter which combines high identification efficiency (at least
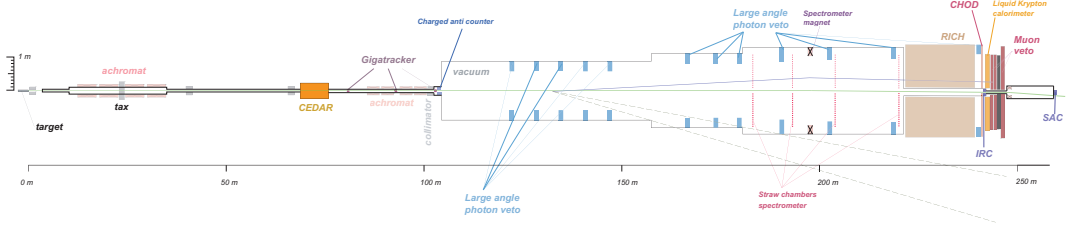
Figure 2. NA62 detector layout.

95%) and excellent time resolution (∼100 ps), as needed for the time matching of a primary and a secondary track. The momentum of beam particles is measured by the beam tracker (Gigatracker, or **GTK**). Each of the three stations of GTK is made of 200 μm thick silicon sensors (300×300 μm size, 0.5 X_0 thickness per station, time resolution better than 200 ps, momentum resolution 0.2%). The detector is operated at ∼750 MHz rate.

The momentum of secondary particles is measured by the Straw chamber spectrometer (**STRAW**). Each of the four STRAW stations comprises 1792 straw tubes arranged in four views (X, Y, U, V) and is operated in vacuum. The achieved momentum resolution is better than 1%.

The **RICH** detector aims at separating secondary pions from muons at the level of 1% (muon contamination in the pion sample) in the momentum range 15–35 GeV/c. A good time resolution (below 100 ps) is necessary both for time matching of two tracks (primary and secondary) and for providing a signal for the L0/L1 trigger. The charged particle hodoscope (**CHOD**) consisting of 128 scintillator slabs arranged in 2 planes (horizontal and vertical) measures the track crossing time with ∼200 ps resolution and also contributes to the L0 trigger.

The photon veto system covers the angular range up to 50 mrad and includes 4 detectors: **LAV** (12 stations operated in vacuum, made of lead glass blocks and covering the angular region from 8.5 to 50 mrad), **LKr** (liquid Krypton calorimeter from the NA48/2 experiment, vetoing the region from 1 to 8.5 mrad), **IRC** and **SAC** (small angle calorimeters covering the angular region <1 mrad). The rejection power of the veto system should be ∼10^8 for decays with π^0 in the final state. The **CHANTI** detector placed after the GTK3 identifies upstream inelastic interactions and muon halo. The iron/scintillator calorimeters (**MUV1**, **MUV2**) provide further pion/muon separation. Together with the RICH, this separation (muon mis-ID) should be ∼10^{-7}. A fast muon veto **MUV3** (iron wall followed by 5 cm thick scintillator, the light is detected by PMs) identifies muons and provides L0 trigger signals.

3 Analysis strategy

The signal detection principles are driven by the low BR of the decay (and hence a huge background), weak experimental signature (one primary and one secondary track) and the required background level (∼10%). This leads to the following strategy:

- high beam intensity and fast timing;
- decays-in-flight technique;
- kinematic reconstruction and efficient particle identification (PID);
- efficient veto system.

The main kinematic variable used in the analysis is the missing mass squared:
$m_{miss}^2 = (P_K - P_\pi)^2 \simeq m_K^2(1 - \frac{|p_\pi|}{|p_K|}) + m_\pi^2(1 - \frac{|p_K|}{|p_\pi|}) - |p_K||p_\pi|\theta_{\pi K}^2$. Here P_K and P_π are kaon and
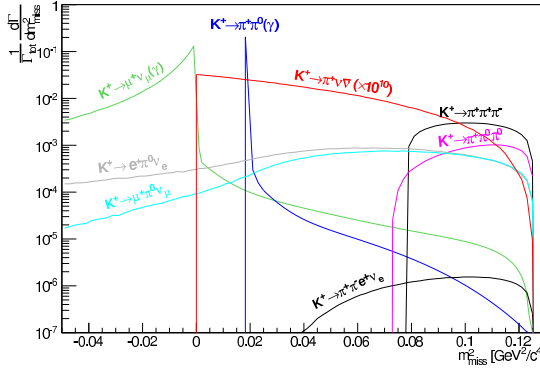
Figure 3. $m_{miss}^2 = (P_K - P_\pi)^2$ for the signal and the most frequent background decay modes. The signal is multiplied by 10^{10}, background modes are normalized according to their BR.

pion 4-momenta, p_K and p_π are their 3-momenta and $\theta_{\pi K}$ is the angle between two particles in the laboratory frame.

Fig. 3 shows the distribution of this variable for the signal and backgrounds. Two signal regions are constrained by the main background from the decays $K^+ \rightarrow \mu^+ \nu_\mu$ (on the left), $K^+ \rightarrow \pi\pi\pi$ (on the right) and $K^+ \rightarrow \pi^+ \pi^0$ (a peak from this decay splits the signal region into 2 halves). Kinematic cuts on the m_{miss}^2 allow to reject ~90% of background events. Further suppression is done by the veto system and PID.

4 Preliminary results of the 2015 run

The main goal of the 2015 run was to check the detector performances and the data quality. The data were collected at low beam intensity (~10% of the nominal), the single-track selection criteria were close to those of the final measurement of the BR($K^+ \rightarrow \pi^+ \nu\bar{\nu}$):

- one primary track in GTK;
- one secondary track in STRAW;
- reconstructed vertex within the decay region;
- energy deposit in LKr;
- hits in the RICH and CHOD;
- spatial matching (STRAW-CHOD, STRAW-LKr);
- time matching (GTK-RICH-CHOD).

The m_{miss}^2 distributions for the 2015 data are shown in Fig. 4. The first distribution is done with a kaon-like signal in the KTAG and demonstrates main backgrounds, while the second one illustrates the main sources of downstream tracks not related to the kaon decays: beam elastic scattering in the material along the beamline (KTAG, GTK) and inelastic scattering in the last GTK station.

Time resolutions of the KTAG and GTK are found to match the design values (100 and 200 ps respectively). The resolution of the m_{miss}^2 is measured using the peak from the $K^+ \rightarrow \pi^+ \pi^0$ decay and
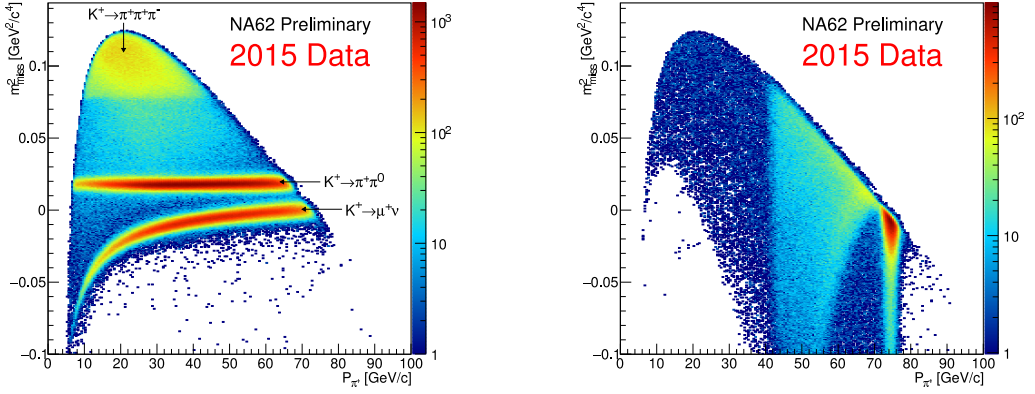
Figure 4. $m_{miss}^2 = (P_K - P_\pi)^2$ vs momentum after single-track event selection for kaon decays (left) and without a kaon tag (right).
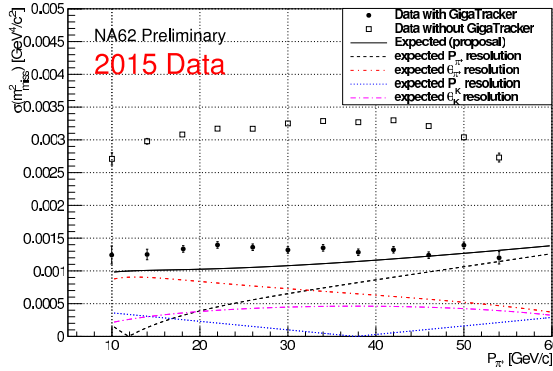

Figure 5. Resolution of the m_{miss}^2 vs momentum. Empty squares correspond to the values obtained with the nominal kaon momentum, black points - with the kaon momentum measured by GTK.

found to be 1.2×10^{-3} close to the design value 10^{-3}. The resolution as a function of momentum is shown in Fig. 5.

The identification of secondary charged particles is done in the RICH detector. Fig. 6 illustrates the dependence of the Cherenkov ring radius on the momentum for the single-track selection. The pion-muon separation is based on the difference in ring radii for π and μ. It was measured by selecting a pure muon sample from $K^+ \to \mu^+ \nu_\mu$ decay and a pion sample from $K^+ \to \pi^+ \pi^0$ decay. In the momentum range between 15 and 35 GeV/c the required muon contamination of 1% was achieved at the 80% pion ID efficiency.

The photon veto system is designed to suppress decays with photons in the final state. For photons from π^0 decays the rejection power provided by LAV, LKr, IRC and SAC detectors should be at least
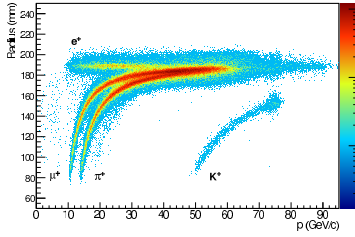
Figure 6. RICH Cherenkov ring radius vs momentum.
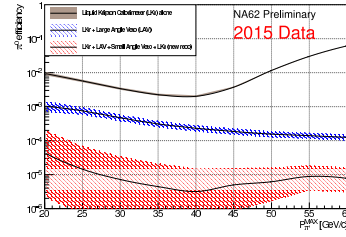
Figure 7. π^0 veto inefficiency for various calorimetric combinations vs momentum.

10^8, or, in other words, the veto inefficiency for photons with energy above 10 GeV should not exceed 10^{-5}. The π^0 veto inefficiency measured from the $K^+ \to \pi^+\pi^0$ decay is shown in Fig. 7. The amount of statistics recorded in 2015 limits this measurement to 10^{-6} (90% CL).

5 Conclusion

The NA62 experiment plans to collect ~100 events of the ultra rare decay $K^+ \to \pi^+ \nu\bar{\nu}$ in 2016–2018. In 2015 run the setup performance was studied using the data collected at low beam intensity. The results demonstrate that the experiment is approaching the design sensitivity.

References

[1] J. Brod, M. Gorbahn and E. Stamou, PRD **83**, 034030 (2011)
[2] A.J. Buras, D. Buttazzo, J. Girrbach-Noe and R. Knegjens, JHEP **1511**, 33 (2015)
[3] M. Blanke, A.J. Buras and S. Recksiegel, Eur. Phys. J. **C76** no.4, 182 (2016)
[4] M. Blanke, A.J. Buras, B. Duiling, K. Gemmler and S. Gori, JHEP **903**, 108 (2009)
[5] A. V. Artamonov *et al.*, PRD **79**, 092004 (2009)
[6] J.K. Ahn *et al.*, PRD **81**, 072004 (2010)
[7] The NA62 collaboration, NA62 Technical Design Document, **NA62-10-07** (2010), https://cds.cern.ch/record/1404985